Investigating the Adsorption/Desorption Kinetics of a Molecular Water Oxidation Catalyst at an Electrode Interface

Boqiang Chen,[†,‡] Hongna Zhang,[†,‡] Ruolin Zhang,[†,‡] Tianying Liu,[†] Dongyoon Shin,[†] Dunwei Wang,[*,†] and Matthias M. Waegele[*,†]

†*Department of Chemistry, Merkert Chemistry Center, Boston College, Chestnut Hill, Massachusetts 02467, United States*
‡*Contributed Equally*

E-mail: dunwei.wang@bc.edu; waegele@bc.edu

Abstract

Probing the dynamics of molecular catalysts at electrode/electrolyte interfaces is essential for understanding catalytic mechanisms. Structure-specific spectroscopic methods are particularly powerful for examining electrocatalytic interfaces but are mostly used under steady-state conditions. Herein, we combined surface-enhanced infrared absorption spectroscopy (SEIRAS) with phase-sensitive detection (PSD) to investigate the dynamics of a molecular Ir-based water oxidation catalyst at a Au/electrolyte interface. We found that the amplitude of the absorbance of the catalyst is anticorrelated to that of interfacial water. This anti-correlation can be understood by the adsorption of the electrooxidized catalyst on the electrode and concurrent displacement of interfacial water. The infrared signals from the interface exhibit an increasing phase-lag with respect to the electrode potential with increasing scan rate of the potential. Kinetic modeling suggests that the potential-dependent adsorption/desorption kinetics of the molecular catalyst on the electrode gives rise to this phase-lag. This study shows that PSD-SEIRAS is a powerful tool for investigating the interfacial dynamics of electrocatalytic systems.

Electrocatalysis is fundamentally enabled by dynamic interactions between diverse chemical species at electrochemical interfaces. The dynamics relevant for electrocatalysis span a wide range of timescales from hours to picoseconds and include the kinetics of adsorption/desorption of interfacial species,[1–3] (de)solvation,[4,5] surface reconstructions,[6–10] and double-layer formation.[11,12] Structure-specific methods, such as vibrational spectroscopy or X-ray techniques, are particularly well-suited to investigate the molecular structure and dynamics of electrochemical interfaces.[13–17] However, probing these dynamic processes with structure-specific methods is often challenging, especially when the transient signals of interest are weak or difficult to discern. Therefore, there is a great need to advance structure-specific methods capable of monitoring dynamic interfacial processes with high detection sensitivity.

Modulation excitation spectroscopy (MES) is a powerful technique that can be combined with different spectroscopic methods to greatly enhance signal-to-noise ratios.[18–21] In MES, the system is excited periodically and its response is monitored as a function of time. Within this context, phase-sensitive detection (PSD) of the time-dependent signal gives rise to the phase-domain response, which has a much higher

signal-to-noise ratio. In addition, the analysis of the phase delay between excitation and response provides information about the kinetics of the underlying processes.[19,22]

In a previous study,[23] we combined surface-enhanced infrared absorption spectroscopy (SEIRAS) with PSD to study a homogeneous Ir catalyst ("blue Ir-dimer"[24]) at a Au electrode/aqueous electrolyte interface. We showed that PSD-SEIRAS is capable of detecting infrared (IR) bands with amplitudes as low as several tens of μOD (OD = optical density). We identified two reaction intermediates, oxo (Ir^{V}=O) and superoxo (Ir^{IV}-$OO^{\bullet}$), whose relative populations change with electrode potential. In our earlier study, however, we did not analyze the phase delay of the IR response with respect to the potential modulation. This analysis is the focus of the present work.

The key motivation for our analysis was the observation that the phase delay between the absorbance from the Ir-dimer increases with increasing scan rate of the electrode potential. A simple kinetic model suggests that the phase delay is likely connected to the adsorption/desorption processes of the electrochemically oxidized Ir-dimer. This hypothesis is supported by how the IR signals of interfacial water and the Ir-dimer respond to the electrode potential. These findings show that PSD-SEIRAS is capable of characterizing the adsorption/desorption kinetics of a molecular catalyst at an electrode under dynamic potential control. Understanding this complex interaction between molecular catalyst and electrode is important because the adsorption of a molecular catalyst on an electrode can alter catalytic rates and mechanisms.[25,26]

In MES, the spectroscopic response of the system to an external periodic perturbation is monitored as a function of time. In the present case, the Au electrode was subjected to a series of cyclic voltammetry (CV) scans from 1.4 to 1.7 V_{RHE} (RHE = reversible hydrogen electrode), and single-beam sample spectra of the Au/electrolyte interface, $S(t)$, were collected every 122 ms. The single-beam spectra were then converted to absorbance according to $A(t) = -10^3 \log_{10}(S(t)/R)$, where R

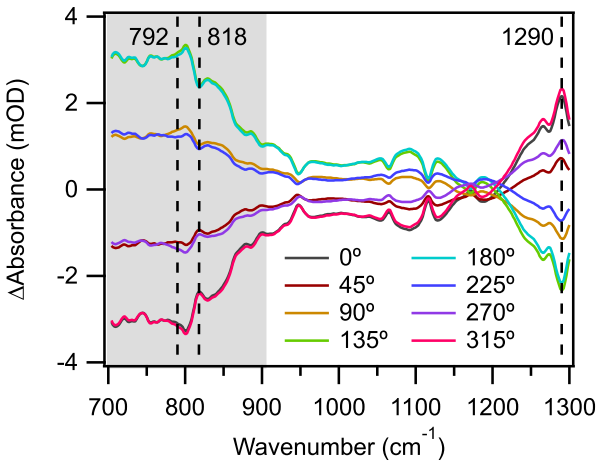

Figure 1: Phase-domain SEIRA spectra of the interface between a polycrystalline Au electrode and an aqueous solution of 0.1 M $HClO_4$ containing 1.25 mM Ir-dimer for different demodulation phase angles, φ^{PSD}, as indicated. The spectra resulted from a modulation of the electrode potential between 1.4 and 1.7 V_{RHE} at a scan rate of 2 mV s^{-1}. The gray highlighted region below 900 cm^{-1} indicates the region of the broad librational band of water. All sharp peaks were ascribed to the active state of Ir-dimer catalyst during water oxidation.

is the single-beam reference spectrum, which was recorded at open circuit. The time-dependent absorbance, $A(t)$, was converted to the phase-domain absorbance using the formula $A_n(\varphi^{PSD}) = \frac{2}{T}\int_0^T A(t)\sin(n\omega t - \pi/2 + \varphi^{PSD})dt$, where T, ω, and φ^{PSD} denote the period, angular frequency, and demodulation phase angle, respectively.[18,19] The term $-\pi/2$ was added because the spectral collection was initiated at the starting potential of the CV (1.4 V_{RHE}), which is the minimum point of the periodic potential modulation. The angular frequency was calculated according to $\omega = \pi\nu/\Delta E$, where ν is the scan rate (in V s^{-1}) and ΔE is the potential range of the CV (in V). Only the first-order response ($n = 1$) yielded a significant signal and is therefore the subject of the following discussion. The second-order response ($n = 2$) did not exhibit pronounced IR signals (Figure S1, Supporting Information). Further details of the data collection and analysis are described in-depth in our previous publication[23] and the

Supporting Information.

Figure 1 shows the phase-domain spectra of the interface between a polycrystalline Au electrode and an aqueous solution of 0.1 M $HClO_4$ containing 1.25 mM Ir-dimer, with the demodulation phase angle shown in the legend. The changes in absorbance were caused by modulating the electrode potential between 1.4 and 1.7 V_{RHE} at a rate of 2 mV s^{-1}. The spectra exhibit a broad band below 900 cm^{-1} (gray-shaded area), which is due to strong water absorptions in this spectral range.[27] In addition to this broad band, there is a series of comparatively sharper bands throughout the observed spectral range. In our previous work,[23] we showed that this series of sharper bands arises from the active state of the Ir-dimer during water oxidation and that the band at 818 cm^{-1} is consistent with an Ir-oxo intermediate. In the present study, we focus on the kinetic information contained in these spectra, which we did not discuss previously.

Inspection of Figure 1 reveals that all sharp bands from the catalyst feature the same phase angle, indicating that they arise from the same species. The broad band below 900 cm^{-1} arises from water librations, that is, hindered rotations of water.[27] The phase of this band is anti-correlated with the sharper bands arising from the active state of the Ir-dimer catalyst: When the absorbance bands from the catalyst increase, there is a loss of absorbance in the water librational band, and vice versa. To understand this anti-correlation between the bands, it is instructive to examine the time-domain data.

Figure 2A shows the absorbance at 792 cm^{-1} during a CV scan. At this wavenumber, the absorbance is dominated by the librational band of interfacial water. In the initial portion of the anodic forward scan, the absorbance is independent of applied potential. Upon reaching a potential of ~1.6 V_{RHE}, the absorbance declines steeply with further increasing electrode potential. This decline coincides with the onset of the water oxidation reaction (Figure S2, Supporting Information). The curve exhibits a substantial hysteresis during the reverse scan, with an initially stable absorbance, followed by a steep rise at ~1.55 V_{RHE}. A control experiment

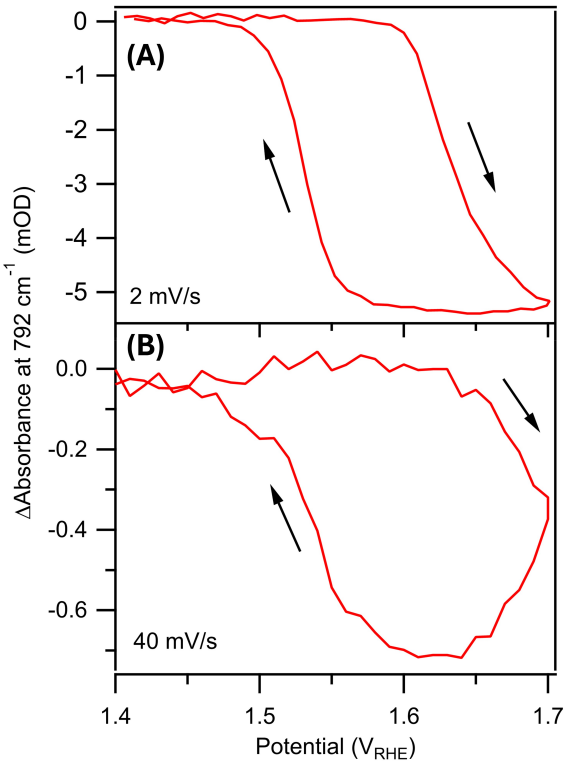

Figure 2: Change of absorbance at 792 cm^{-1} (water librations) on a polycrystalline Au electrode in contact with 0.1 M $HClO_4$ containing 1.25 mM Ir-dimer during a CV between 1.4 and 1.7 V_{RHE} at a scan rate of (A) 2 mV s^{-1} and (B) 40 mV s^{-1}. The arrows indicate the directions of the potential scan.

without the Ir-dimer catalyst in solution, as reported in our previous study,[23] demonstrates that the behavior of the water librational band is not due to the oxidation of Au. Indeed, this potential-dependent profile is suggestive of an electrosorption process[28] and leads to the following hypothesis: Upon passing the potential of ~1.6 V_{RHE}, the Ir-dimer catalyst is oxidized and the oxidized form of the catalyst adsorbs on the electrode, displacing interfacial water. The adsorption of the rather bulky Ir-dimer may displace multiple water layers and/or restructure interfacial water.

It has been reported that redox couples in solution have different formal potentials compared to those of their heterogeneous counterparts for molecular catalysts[26] and self-assembled monolayers.[29] The physicochemical origins include ligation effects,[26] interactions

with electrolyte anions,[30] and differences in local dielectric constant.[31] Therefore, it is conceivable that the adsorbed form of the Ir-dimer catalyst has a different redox potential relative to the catalyst in solution, explaining the hysteresis of the curve in Figure 2A. This interpretation is consistent with the absorbance profile and explains the anti-correlation between the librational band of water and the bands of the Ir-dimer catalyst.

To further strengthen our interpretation, we also examined the absorbance profiles of the O-H stretching and water bending modes (Figures S3-S5, Supporting Information). Both bands exhibited the same behavior as that of the librational band, which further supports the hypothesis of the presence of adsorption/desorption processes in our system. Additional support comes from a control experiment that shows that the reduced species of the Ir-dimer catalyst is not detectable under our experimental conditions (Figure S6, Supporting Information). In our previous study,[23] we also showed that ex-situ X-ray photoelectron spectroscopy (XPS) of the electrode after the SEIRAS experiments reveals the presence of adsorbed Ir-dimer catalyst. The adsorbed species is likely an intact form of the catalyst.[32] A detailed discussion is provided in Supplementary Note 1 of the Supporting Information. However, the chemical nature of the adsorption is not resolved and requires additional research. It is possible that the formation of an oxide layer on Au induces the substitution of H_2O ligands of the Ir-dimer, facilitating its adsorption on the electrode.[33]

With this understanding established, we now examine the dependence of the absorbance profile on the scan rate of the potential. Figure 2B shows the absorbance profile at 792 cm^{-1} for a scan rate of 40 mV s^{-1}. Similar to its behavior at 2 mV s^{-1}, the absorbance does not change substantially until the potential surpasses ~1.6 V_{RHE}, at which point it decreases steeply. Interestingly, upon reversal of the scan direction at 1.7 V_{RHE}, the absorbance continues to decline, in stark contrast to the behavior at 2 mV s^{-1}. Similarly, the O-H stretching and water bending modes exhibited an analogous behavior at a scan rate of 40 mV s^{-1} (Figure S5B,D, Supporting Information). This observation indicates that the physical or chemical processes that control the rates of adsorption/desorption fall behind the rate at which the potential is modulated. The absorbance at 792 cm^{-1} during the CVs for different scan rates from 10 to 80 mV s^{-1} is shown in Figure S7 of the Supporting Information; an overlay of the data for all scan rates is presented in Figure S8 of the Supporting Information.

We note that stochastic simulations show that a reversible, homogeneous process of the form $C_{ox} + e^- \rightleftharpoons C_{red}$ produces a symmetrical concentration profile around the anodic turning potential (Figure S9, Supporting Information), indicating that the different degrees of accumulation/depletion of redox active species at the interface for different scan rates during this process cannot reproduce the experimentally observed phase delay. Details of the simulation are provided further below and in the Supporting Information. Similar results are also obtained from analytical models of the concentrations of electroactive species in the vicinity of the electrode during CV.[34] These findings further support our notion that the origin of the phase delay is related to adsorption/desorption processes involving the electroactive species.

The delay between the potential perturbation and the adsorption/desorption of the Ir-dimer catalyst on the electrode can be quantified using MES. Figure 1 shows that the absorbance at 1290 cm^{-1} is anticorrelated with that arising from water librations (absorbance at 792 cm^{-1}). Accordingly, the absorbance at 1290 cm^{-1} is dominated by the adsorbed Ir-dimer catalyst and will be used to characterize the adsorption/desorption kinetics of the Ir-dimer catalyst. Figure 3 shows the phase delay (ϕ) between the electrode potential and the absorbance at 1290 cm^{-1} (blue trace). The phase delay was calculated using $\phi = 2\pi - \varphi_{max}^{PSD}$, where φ_{max}^{PSD} refers to the demodulation phase angle at which $A_n(\varphi^{PSD})$ reaches its maximum value (Figure S10, Supporting Information). The phase delay changes markedly with the angular frequency of the potential modulation, confirming the observation that the processes that give rise to the signal do not keep up with

the potential-modulation with increasing scan rate. This analysis also confirms that the absorbance of the adsorbed Ir-dimer catalyst is phase shifted by $\sim\pi$ with respect to the absorbance of water at 792 cm^{-1} (Figure S11, Supporting Information), as asserted earlier from qualitative inspection of Figure 1.

To exclude the possibility that the phase delay originates from an instrumental artifact, we conducted vibrational Stark spectroscopy of an electrode decorated with 4-mercaptobenzonitrile (Figure S12, Supporting Information).[35,36] A detailed analysis of the Stark shift is provided in Figures S13 and S14 of the Supporting Information. On the timescale of our experiments, the Stark shift of the nitrile stretching mode of 4-mercaptobenzonitrile is instantaneous and should therefore be independent of the scan rate of the potential. Consistent with this expectation, the Stark shift does not exhibit a phase delay (beige trace in Figure 3), confirming that the phase delay observed for the catalytic system arises from its intrinsic properties.

To confirm that the proposed model can give rise to the observed phase delays and scan-rate dependent absorbance profiles, we built a simple reaction model and examined its kinetic behavior with Kinetiscope, a stochastic kinetics simulator.[37] A schematic of the model is shown in Figure 4A. The model includes a fast single-electron transfer reaction involving the reduced form of the Ir-dimer, C_{red}, and its oxidized form, C_{ox}, in solution and a related process for the corresponding surface-adsorbed species, denoted with a star (*). The only species that is experimentally detectable in our experiments is $^*C_{ox}$, whose formation is assumed to displace interfacial water. The redox reactions of the species in solution and on the surface are assumed to have different equilibrium potentials. This assumption is justified based on the ob-

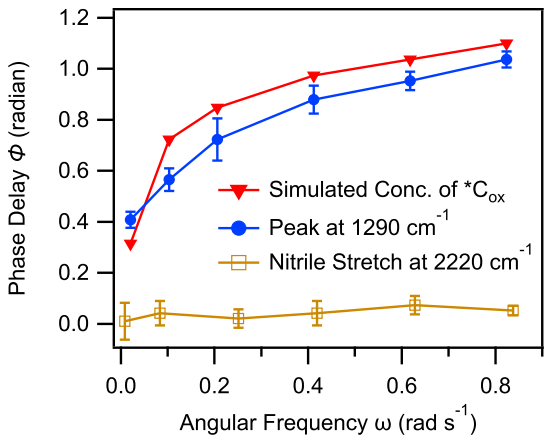

Figure 3: Phase delay of the peak at 1290 cm^{-1}, simulated concentration of $^*C_{ox}$, and integrated area of the nitrile stretching band of 4-mercaptobenzonitrile at 2220 cm^{-1} as a function of angular frequency of the potential modulation. $^*C_{ox}$ refers to the oxidized form of the surface-adsorbed catalyst. Error bars represent standard deviations of the average of 3 independent experiments.

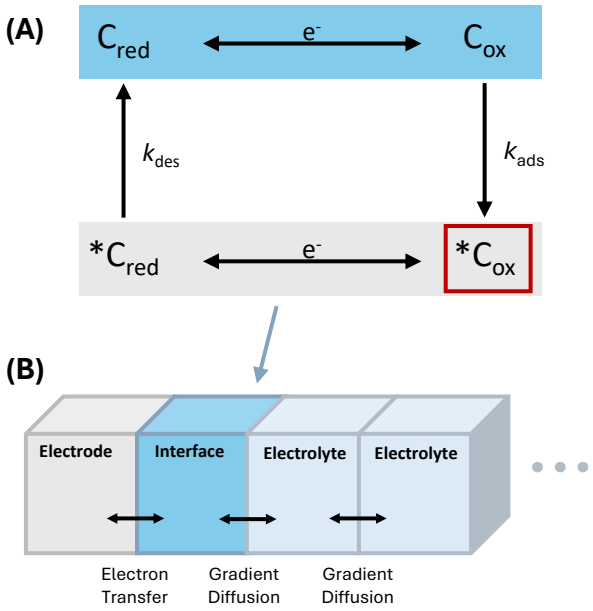

Figure 4: (A) Hypothesized reaction steps at the interface. They include irreversible adsorption and desorption and reversible single-electron transfer. These steps give rise to the interconversion of the reduced and oxidized forms of the catalyst. The gray and dark blue rectangles represent the electrode surface and solution, respectively. The experimentally detected species is highlighted with a red box. (B) Schematic of the simulation system, illustrating the division of the system into a stack of reaction compartments. Electron transfer and gradient diffusion are illustrated by bidirectional arrows.

Table 1: Parameters for kinetic simulation model: equilibrium potentials for the solution and surface redox couples $E_{0,\mathrm{sol}}$ and $E_{0,\mathrm{surf}}$, respectively; standard rate constant of electron transfer k_0; adsorption rate constant k_{ads}; desorption rate constant k_{des}; diffusion coefficient D of solution species.

Parameter	**Value**
$E_{0,\mathrm{sol}}$ ($\mathrm{V_{RHE}}$)	1.65
$E_{0,\mathrm{surf}}$ ($\mathrm{V_{RHE}}$)	1.40
k_0 ($\mathrm{cm\ s^{-1}}$)	0.05
k_{ads} ($\mathrm{M^{-1}s^{-1}}$)	100
k_{des} ($\mathrm{s^{-1}}$)	50
D ($\mathrm{cm^2\ s^{-1}}$)	$0.763 \cdot 10^{-5}$

servation of hysteresis in the adsorption profile (Figure 2A), which was obtained at a slow scan rate (2 mV $\mathrm{s^{-1}}$; quasi-steady state). The oxidized catalyst in solution, $\mathrm{C_{ox}}$, adsorbs irreversibly on the electrode with a rate constant k_{ads}. The reduced form of the surface-adsorbed catalyst, $^*\mathrm{C_{red}}$, desorbs irreversibly with a rate constant k_{des}. The latter assumption of irreversible desorption is justified based on the observation that $^*\mathrm{C_{red}}$ is not detectable in our experiments (Figure S6, Supporting Information). Detection of $^*\mathrm{C_{ox}}$ suggests a sizable equilibrium constant of adsorption, which is given by the ratio of the adsorption rate constant to the desorption rate constant of the oxidized species. Because of limited information about the system, we made the simplifying assumption of an irreversible adsorption process.

Within Kinetiscope, the system was modeled as a stack of reaction compartments (Figure 4B). A more detailed reaction scheme for the simulation is shown in Figure S15 of the Supporting Information. Between electrode and the first electrolyte compartment labeled "interface", only electron transfer was permitted with rates described by the Butler-Volmer model (k_0, E_0, and electrode potential; a symmetry factor of 0.5 was assumed, see Table 1 for definition of symbols). The "interface" compartment contained adsorption sites with a concentration of 0.1 M. The initial concentration of $\mathrm{C_{red}}$ was 1.25 mM in the "interface" and all "electrolyte" compartments. $\mathrm{C_{red}}$ and $\mathrm{C_{ox}}$ were free to diffuse between all compartments but the one labeled "electrode". Details of the simulation are described in the Supporting Information.

The simulation parameters were altered until good agreement with the experimental results was achieved. The chosen parameters are shown in Table 1 and a description of how they were determined is provided in the Supporting Information. The kinetic scheme and parameters lead to a negligible surface-concentration of $^*\mathrm{C_{red}}$ (Figure S16, Supporting Information), consistent with the experimental observation of only a single surface species. In addition, the simulated concentrations of the solution species $\mathrm{C_{ox}}$ and $\mathrm{C_{red}}$ near the electrode surface do not exhibit a phase delay with respect to the scan rate of the electrode potential (Figures S17 and S18, Supporting Information), which further supports our proposed model that the observed phase delay arises from adsorption/desorption of surface species.

Figure 5 compares the simulated concentration of $^*\mathrm{C_{ox}}$ (red traces, left ordinates) with the absorbance of the adsorbed Ir-dimer catalyst (probed at 1290 $\mathrm{cm^{-1}}$; blue traces, right ordinates) as a function of time for different scan rates from 2 to 80 mV $\mathrm{s^{-1}}$. The simulated profiles reproduce the trends in the experimental ones. Inspection of Figure 3 shows that the phase delay between electrode potential and the simulated concentration of $^*\mathrm{C_{ox}}$ qualitatively follows the experimental data (peak amplitude at 1290 $\mathrm{cm^{-1}}$). We note that the kinetic model does not capture the full complexity of the real system, which involves multiple electron/proton-transfers and turnover of the oxidized catalyst from water oxidation. Therefore, the values of the parameters in Table 1 should not be quantitatively interpreted. Irrespective of these apparent limitations, the model supports our hypothesis that the delay between potential perturbation and infrared signal arises from the potential-induced adsorption/desorption kinetics of the Ir-dimer catalyst on the electrode.

To test the robustness of this interpretation, we examined the sensitivity of the model to the

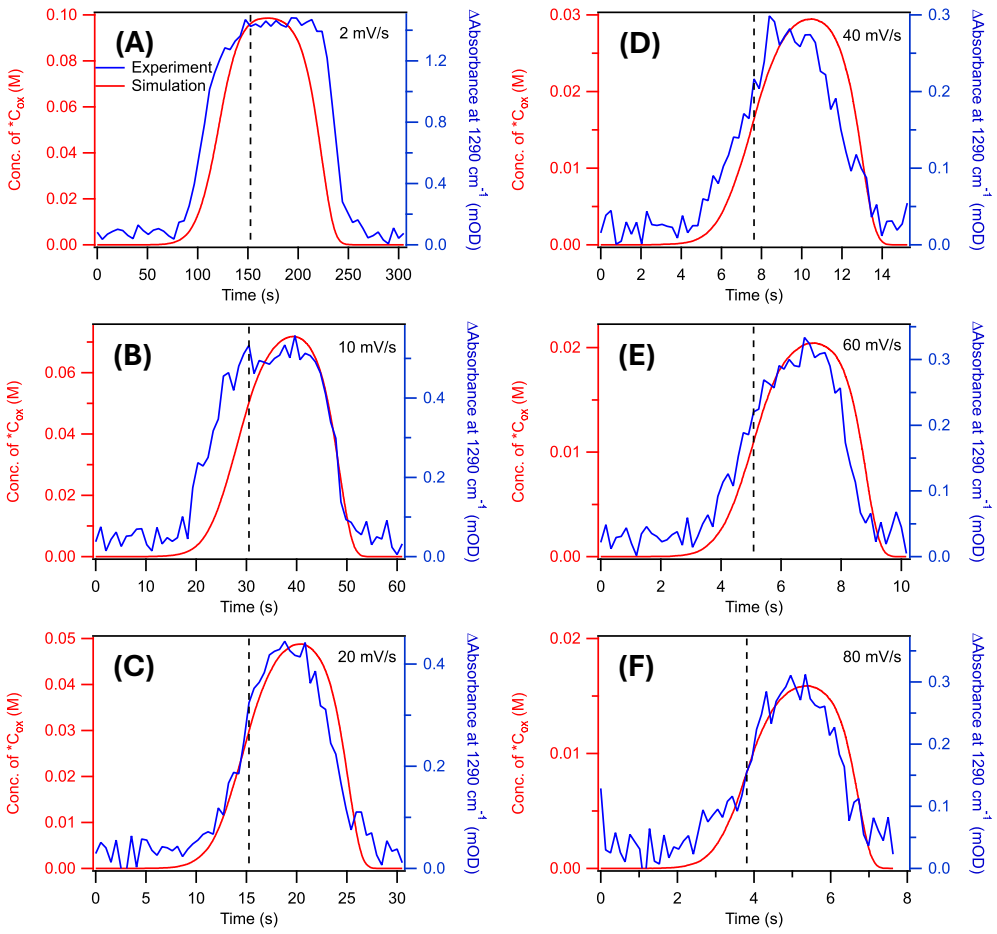

Figure 5: Comparison between the simulated concentration of $^*C_{ox}$ (red) and the experimentally measured absorbance at 1290 cm^{-1} (blue) as a function of time for the potential scan rates of (A) 2, (B) 10, (C) 20, (D) 40, (E) 60, and (F) 80 mV s^{-1}. The dashed line in each panel represents the anodic turning potential of the CV (1.7 V_{RHE}).

model parameters and considered an alternative kinetic scheme. First, we systematically examined the response of the phase lag to the model parameters $E_{0,\mathrm{sol}}$, $E_{0,\mathrm{surf}}$, k_{ads}, and k_{des}. As shown in Figure S19 of the Supporting Information, the value of the phase delay displays sensitivity to all model parameters but is most sensitive to the parameters that control desorption of $^*C_{ox}$ ($E_{0,\mathrm{surf}}$, k_{des}). However, the change of the delay with increasing scan rate is relatively insensitive to the choice of the model parameters. Second, we examined a model that includes a reaction channel in which the oxidized species, C_{ox} and $^*C_{ox}$, decay in a potential-independent manner due to water nucleophilic attack. This step is often assumed to be rate-limiting in the oxidation of water.[38–40] This alternative scenario that includes potential-independent turnover of $C_{ox}/^*C_{ox}$ due to water nucleophilic attack does not change the qualitative features of the model (Figures S20 and S21, Table S1, Supporting Information). These observations confirm the robustness of our model in qualitatively explaining the experimentally observed phase delay.

In summary, during MES of the interface of a Au electrode and an electrolyte containing a molecular water oxidation catalyst (Ir-dimer), we observed two infrared signals whose amplitudes are anticorrelated. As established in our previous work,[23] one signal is attributable to librations of interfacial water, the other to the active state of the Ir-dimer catalyst at the interface. Herein, we showed that the anticorrelation of the two signals can be understood by the adsorption of the oxidized form of the Ir-

dimer on the Au electrode and the associated displacement of interfacial water from the electrode. Further evidence for this interpretation comes from the potential-dependent absorbance profiles, which suggest an electrosorption process. We further showed that the phase-shifts of the IR signals with respect to the periodic potential modulation increase with increasing scan rate of the electrode potential, indicating that the physical and/or chemical processes that underlie the infrared signal fall behind the potential-modulation frequency. A simplified kinetic model of the catalyst system implicates the potential-driven adsorption/desorption of the Ir-dimer as a possible origin of the phase delay. Our study shows that PSD-SEIRAS has the potential to reveal interfacial dynamics of complex electrocatalytic systems.

Supporting Information. Experimental procedures; discussion the molecular nature of the adsorbed species; phase-domain SEIRA spectra (second-order response); CV of Au in contact with Ir-dimer solution; phase-domain SEIRA spectra over a wider range of wavenumbers; steady-state spectra collected in Ir-dimer solution; absorbance changes of water librational, stretching and bending modes during potential modulation; phase-domain SEIRA spectra for a potential modulation between 1.3 and 1.6 V_{RHE}; change of absorbance of water librations as a function of potential for different scan rates; simulation for reversible one-electron transfer; peak amplitude at 1290 cm^{-1} versus demodulation phase angle; phase delay of water librational band; phase-domain and time-domain SEIRA spectra of 4-mercaptobenzonitrile on Au; explanation of biphasic nitrile stretching band; detailed scheme of simulation; simulated concentration profiles of all solution and surface species (C_{red}, C_{ox}, $*C_{red}$, and $*C_{ox}$); dependence of phase delay on simulation parameters; alternative model, including decay of C_{ox} and $*C_{ox}$ due to water oxidation.

Acknowledgement This work was supported by the U.S. Department of Energy (DOE), Office of Science, Office of Basic Energy Sciences, Chemical Sciences, Geosciences, and Biosciences Division under contract DE-SC0020261. We thank Professor Cyrille Costentin for helpful discussions.

References

(1) Unwin, P. R.; Bard, A. J. Scanning Electrochemical Microscopy. 14. Scanning Electrochemical Microscope Induced Desorption: A New Technique for the Measurement of Adsorption/Desorption Kinetics and Surface Diffusion Rates at the Solid/Liquid Interface. *J. Phys. Chem.* **1992**, *96*, 5035–5045.

(2) Climent, V.; Coles, B. A.; Compton, R. G. Coulostatic Potential Transients Induced by Laser Heating of a Pt(111) Single-Crystal Electrode in Aqueous Acid Solutions. Rate of Hydrogen Adsorption and Potential of Maximum Entropy. *J. Phys. Chem.B* **2002**, *106*, 5988–5996.

(3) Lin, C.; Jiao, X.; Tschulik, K.; Batchelor-McAuley, C.; Compton, R. G. Influence of Adsorption Kinetics upon the Electrochemically Reversible Hydrogen Oxidation Reaction. *J. Phys. Chem. C* **2015**, *119*, 16121–16130.

(4) Yamakata, A.; Soeta, E.; Ishiyama, T.; Osawa, M.; Morita, A. Real-Time Observation of the Destruction of Hydration Shells under Electrochemical Force. *J. Am. Chem. Soc.* **2013**, *135*, 15033–15039.

(5) Maitra, A.; Pennathur, A. K.; Chiang, P.-H.; Dawlaty, J. M. Direct Spectroscopic Observation of Ultraslow Ion Desolvation at an Interface. *ACS Appl. Energy Mater.* **2024**, *7*, 5528–5536.

(6) Matsushima, H.; Taranovskyy, A.; Haak, C.; Gründer, Y.; Magnussen, O. M. Reconstruction of Cu(100) Electrode Surfaces during Hydrogen Evolution. *J. Am. Chem. Soc.* **2009**, *131*, 10362–10363.

(7) Jeon, H. S.; Timoshenko, J.; Rettenmaier, C.; Herzog, A.; Yoon, A.;

Chee, S. W.; Oener, S.; Hejral, U.; Haase, F. T.; Roldan Cuenya, B. Selectivity Control of Cu Nanocrystals in a Gas-Fed Flow Cell through CO_2 Pulsed Electroreduction. *J. Am. Chem. Soc.* **2021**, *143*, 7578–7587.

(8) Edgington, J.; Vicente, R.; Vispute, S.; Li, R.; Sweers, M. E.; Sullivan, S. R.; Fernandez, P. S.; Seitz, L. C. Dynamics of Highly Active Ln_3IrO_7 Catalysts for the Oxygen Evolution Reaction in Acid. *Adv. Energy Mater.* **2024**, *14*, 2402333.

(9) Liu, Q.; Zang, J.; Ye, W.; Li, L.; Wang, C.; Jin, J.; Yang, W. Universal Formation, Dynamics, and Reactivities of $*CO_{bridge}$ Accompanying Spontaneous Reconstruction of Cu during Electrochemical CO_2 or CO Reduction. *J. Am. Chem. Soc.* **2025**, *147*, 31497–31508.

(10) Rebstock, J. A.; Rao, A.; Samanta, A.; Asthagiri, A.; Baker, L. R. Specifically Adsorbed Carbonate Ions and Copper Surface Reconstruction: The Effect of Double Layer Charging Revealed by Time-Resolved Sum Frequency Generation Spectroscopy. *J. Am. Chem. Soc.* **2025**, *147*, 41404–41412.

(11) Yamakata, A.; Osawa, M. Dynamics of Double-Layer Restructuring on a Platinum Electrode covered by CO: Laser-Induced Potential Transient Measurement. *J. Phys. Chem. C* **2008**, *112*, 11427–11432.

(12) Greco, A.; Imoto, S.; Backus, E. H. G.; Nagata, Y.; Hunger, J.; Bonn, M. Ultrafast Aqueous Electric Double Layer Dynamics. *Science* **2025**, *388*, 405–410.

(13) van Oversteeg, C. H. M.; Doan, H. Q.; de Groot, F. M. F.; Cuk, T. In Situ X-Ray Absorption Spectroscopy of Transition Metal Based Water Oxidation Catalysts. *Chem. Soc. Rev.* **2017**, *46*, 102–125.

(14) Kas, R.; Ayemoba, O.; Firet, N. J.; Middelkoop, J.; Smith, W. A.; Cuesta, A. In-Situ Infrared Spectroscopy Applied to the Study of the Electrocatalytic Reduction of CO_2: Theory, Practice and Challenges. *ChemPhysChem* **2019**, *20*, 2904–2925.

(15) Chang, X.; Vijay, S.; Zhao, Y.; Oliveira, N. J.; Chan, K.; Xu, B. Understanding the Complementarities of Surface-Enhanced Infrared and Raman Spectroscopies in CO Adsorption and Electrochemical Reduction. *Nat. Commun.* **2022**, *13*, 2656.

(16) Wang, J.; Liu, M.-T.; Hsu, C.-S.; Chu, Y.-C.; Liao, Y.-F.; Pao, C.-W.; Chan, T.-S.; Chuang, W.-T.; Chen, J.-L.; Shao, Y.-C.; Ishii, H.; Hiraoka, N.; Chiang, C.-Y.; Chen, H. M. Resolving Dynamic Behavior of Electrocatalysts via Advances of Operando X-Ray Absorption Spectroscopies: Potential Artifacts and Practical Guidelines. *Adv. Mater.* **2025**, *37*, 2418797.

(17) Ge, A.; Rudshteyn, B.; Videla, P. E.; Miller, C. J.; Kubiak, C. P.; Batista, V. S.; Lian, T. Heterogenized Molecular Catalysts: Vibrational Sum-Frequency Spectroscopic, Electrochemical, and Theoretical Investigations. *Acc. Chem. Res.* **2019**, *52*, 1289–1300.

(18) Baurecht, D.; Fringeli, U. P. Quantitative Modulated Excitation Fourier Transform Infrared Spectroscopy. *Rev. Sci. Instrum.* **2001**, *72*, 3782–3792.

(19) Urakawa, A.; Bürgi, T.; Baiker, A. Sensitivity Enhancement and Dynamic Behavior Analysis by Modulation Excitation Spectroscopy: Principle and Application in Heterogeneous Catalysis. *Chem. Eng. Sci.* **2008**, *63*, 4902–4909.

(20) Ferri, D.; Newton, M. A.; Nachtegaal, M. Modulation Excitation X-Ray Absorption Spectroscopy to Probe Surface Species on Heterogeneous Catalysts. *Top. Catal.* **2011**, *54*, 1070.

(21) Czioska, S.; Boubnov, A.; Escalera-López, D.; Geppert, J.; Zagalskaya, A.;

Röse, P.; Saraçi, E.; Alexandrov, V.; Krewer, U.; Cherevko, S.; Grunwaldt, J.-D. Increased Ir-Ir Interaction in Iridium Oxide During the Oxygen Evolution Reaction at High Potentials Probed by Operando Spectroscopy. *ACS Catal.* **2021**, *11*, 10043–10057.

(22) Eigen, M. Methods for Investigation of Ionic Reactions in Aqueous Solutions with Half-Times as Short as 10^{-9} Sec. Application to Neutralization and Hydrolysis Reactions. *Discuss. Faraday Soc.* **1954**, *17*, 194–205.

(23) Zhang, H.; Chen, B.; Liu, T.; Brudvig, G. W.; Wang, D.; Waegele, M. M. Infrared Spectroscopic Observation of Oxo- and Superoxo-Intermediates in the Water Oxidation Cycle of a Molecular Ir Catalyst. *J. Am. Chem. Soc.* **2024**, *146*, 878–883.

(24) Volpe, A.; Tubaro, C.; Natali, M.; Sartorel, A.; Brudvig, G. W.; Bonchio, M. Light-Driven Water Oxidation with the Ir-blue Catalyst and the $Ru(bpy)_3^{2+}/S_2O_8^{2-}$ Cycle: Photogeneration of Active Dimers, Electron-Transfer Kinetics, and Light Synchronization for Oxygen Evolution with High Quantum Efficiency. *Inorg. Chem.* **2019**, *58*, 16537–16545.

(25) Sathrum, A. J.; Kubiak, C. P. Kinetics and Limiting Current Densities of Homogeneous and Heterogeneous Electrocatalysts. *J. Phys. Chem. Lett.* **2011**, *2*, 2372–2379.

(26) Costentin, C.; Dridi, H.; Savéant, J.-M. Molecular Catalysis of O_2 Reduction by Iron Porphyrins in Water: Heterogeneous versus Homogeneous Pathways. *J. Am. Chem. Soc.* **2015**, *137*, 13535–13544.

(27) Giguère, P. A.; Harvey, K. B. On the Infrared Absorption of Water and Heavy Water in Condensed States. *Can. J. Chem.* **1956**, *34*, 798–808.

(28) Gileadi, E. *Physical Electrochemistry, 1st Ed.*; Wiley-VCH, 2011.

(29) Song, S.; Clark, R. A.; Bowden, E. F.; Tarlov, M. J. Characterization of Cytochrome c/Alkanethiolate Structures Prepared by Self-Assembly on Gold. *J. Phys. Chem.* **1993**, *97*, 6564–6572.

(30) Rudnev, A. V.; Zhumaev, U.; Utsunomiya, T.; Fan, C.; Yokota, Y.; ichi Fukui, K.; Wandlowski, T. Ferrocene-Terminated Alkanethiol Self-Assembled Monolayers: An Electrochemical and In Situ Surface-Enhanced Infra-Red Absorption Spectroscopy Study. *Electrochim. Acta* **2013**, *107*, 33–44.

(31) Smith, C. P.; White, H. S. Theory of the interfacial potential distribution and reversible voltammetric response of electrodes coated with electroactive molecular films. *Anal. Chem.* **1992**, *64*, 2398–2405.

(32) Hetterscheid, D. G. H.; van der Ham, C. J. M.; Diaz-Morales, O.; Verhoeven, M. W. G. M. T.; Longo, A.; Banerjee, D.; Niemantsverdriet, J. W. H.; Reek, J. N. H.; Feiters, M. C. Early Stages of Catalyst Aging in the Iridium Mediated Water Oxidation Reaction. *Phys. Chem. Chem. Phys.* **2016**, *18*, 10931–10940.

(33) Sheehan, S. W.; Thomsen, J. M.; Hintermair, U.; Crabtree, R. H.; Brudvig, G. W.; Schmuttenmaer, C. A. A Molecular Catalyst for Water Oxidation that Binds to Metal Oxide Surfaces. *Nat. Commun.* **2015**, *6*, 6469.

(34) Bard, A.; Faulkner, L.; White, H. *Electrochemical Methods: Fundamentals and Applications*; Wiley, 2022.

(35) Sarkar, S.; Maitra, A.; Banerjee, S.; Thoi, V. S.; Dawlaty, J. M. Electric Fields at Metal–Surfactant Interfaces: A Combined Vibrational Spectroscopy and Capacitance Study. *J. Phys. Chem. B* **2020**, *124*, 1311–1321.

(36) Delley, M. F.; Nichols, E. M.; Mayer, J. M. Interfacial Acid–Base Equilibria and Electric Fields Concurrently Probed by In Situ

Surface-Enhanced Infrared Spectroscopy. *J. Am. Chem. Soc.* **2021**, *143*, 10778–10792.

(37) Wiegel, A. A.; Wilson, K. R.; Hinsberg, W. D.; Houle, F. A. Stochastic Methods for Aerosol Chemistry: A Compact Molecular Description of Functionalization and Fragmentation in the Heterogeneous Oxidation of Squalane Aerosol by OH Radicals. *Phys. Chem. Chem. Phys.* **2015**, *17*, 4398–4411.

(38) Surendranath, Y.; Kanan, M. W.; Nocera, D. G. Mechanistic Studies of the Oxygen Evolution Reaction by a Cobalt-Phosphate Catalyst at Neutral pH. *J. Am. Chem. Soc.* **2010**, *132*, 16501–16509.

(39) Gerken, J. B.; McAlpin, J. G.; Chen, J. Y. C.; Rigsby, M. L.; Casey, W. H.; Britt, R. D.; Stahl, S. S. Electrochemical Water Oxidation with Cobalt-Based Electrocatalysts from pH 0–14: The Thermodynamic Basis for Catalyst Structure, Stability, and Activity. *J. Am. Chem. Soc.* **2011**, *133*, 14431–14442.

(40) Ping, Y.; Nielsen, R. J.; Goddard, W. A. The Reaction Mechanism with Free Energy Barriers at Constant Potentials for the Oxygen Evolution Reaction at the IrO_2 (110) Surface. *J. Am. Chem. Soc.* **2017**, *139*, 149–155.

TOC Graphic

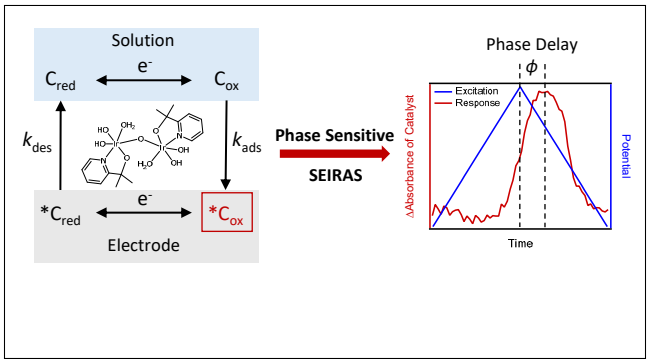
Solution
e-
Cred
Cox
kdes
kads
*Cred
e-
*Cox
Electrode
Phase Sensitive
SEIRAS
Phase Delay
ϕ
Excitation
Response
ΔAbsorbance of Catalyst
Potential
Time